Experimental and Theoretical Analysis of Fast Lithium Ionic Conduction in a LiBH 4 −C 60 Nanocomposite

ARTICLE *in* THE JOURNAL OF PHYSICAL CHEMISTRY C · SEPTEMBER 2014

Impact Factor: 4.77 · DOI: 10.1021/jp503797s

10 AUTHORS, INCLUDING:

Joseph Teprovich
Savannah River National Laboratory
27 PUBLICATIONS **223** CITATIONS
SEE PROFILE

Jian Zhou
Virginia Commonwealth University
41 PUBLICATIONS **1,041** CITATIONS
SEE PROFILE

Robert Compton
University of Tennessee
316 PUBLICATIONS **7,005** CITATIONS
SEE PROFILE

THE JOURNAL OF PHYSICAL CHEMISTRY C

Article

pubs.acs.org/JPCC

Experimental and Theoretical Analysis of Fast Lithium Ionic Conduction in a $LiBH_4$–C_{60} Nanocomposite

Joseph A. Teprovich, Jr.,[†] Héctor R. Colón-Mercado,[†] Patrick A. Ward,[†,‡] Brent Peters,[†] Santanab Giri,[§] Jian Zhou,[§] Scott Greenway,[∥] Robert N. Compton,[‡] Purusottan Jena,[§] and Ragaiy Zidan*[,†]

[†]Savannah River National Laboratory, Clean Energy Directorate, Aiken, South Carolina 29808, United States

[‡]Department of Chemistry, University of Tennessee, Knoxville, Tennessee 37996, United States

[§]Physics Department, Virginia Commonwealth University, Richmond, Virginia 23284, United States

[∥]Applied Research Center, Savannah River Site, 301 Gateway Drive, Aiken, South Carolina 29808, United States

Supporting Information

ABSTRACT: We have developed a $LiBH_4$–C_{60} nanocomposite that displays fast lithium ionic conduction in the solid state. The material is a homogeneous nanocomposite that contains both $LiBH_4$ and a hydrogenated fullerene species. In the presence of C_{60}, the lithium ion mobility of $LiBH_4$ is significantly enhanced in the as-prepared state when compared to pure $LiBH_4$. We also observed that after the material is annealed, the lithium ion mobility is further enhanced. The magnitude of enhancement in lithium ion mobility of the annealed material is comparable to that previously observed for LiX (X = halide) addition to $LiBH_4$. In a $LiBH_4$:C_{60} 70:30 wt % sample that was annealed, we measured Li ionic conductivity of 2.0×10^{-5} S/cm at 25 °C and 2.0×10^{-3} S/cm at 140 °C. Constant current cycling demonstrated that the material is stable in the presence of metallic lithium electrodes. First-principles calculations were also performed to demonstrate how C_{60} perturbs the interaction of lithium with the borohydride anion yielding a plausible explanation for the observed high ionic conductivity. The feasibility of this material as a solid state electrolyte was then demonstrated in a solid-state lithium ion battery.

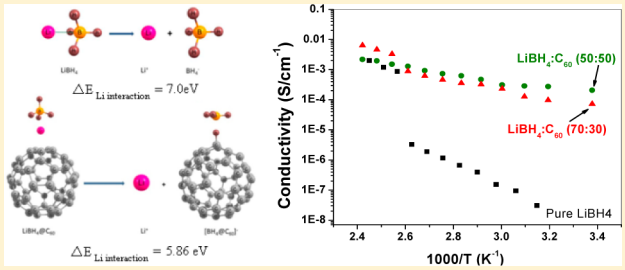

1. INTRODUCTION

Complex metal hydrides ($NaAlH_4$, $LiAlH_4$, $LiBH_4$, etc.) have been extensively evaluated for their hydrogen storage properties. However, these materials do not currently meet the U.S. Department of Energy (DOE) requirements for solid-state onboard vehicular hydrogen storage. As a result, researchers began to evaluate the physical and chemical properties of complex metal hydrides to determine whether they could be utilized as components in other energy storage and conversion devices. This led to the seminal work of the Orimo group, which successfully demonstrated that $LiBH_4$ has the potential to be utilized as a fast lithium ionic conductor.[1] $LiBH_4$ undergoes a structural phase change (occurring at ∼390 K) from orthorhombic to hexagonal upon heating. The high temperature phase (hexagonal) has a conductivity of 10^{-3} S cm^{-1} while the low temperature phase (orthorhombic) has between 10^{-8} and 10^{-6} S cm^{-1}. Additionally, the phase transition from orthorhombic to hexagonal results in a lowering of the activation energy required for conduction from 0.69 to 0.53 eV. Since this work, it has been demonstrated that the introduction of inorganic salts, anions, and metal dopants can significantly enhance the mobility of the Li ion in the solid state.[2−9] The Li ion conductivity in various metal hydrides has also been reviewed by Orimo.[10] A recent report has also demonstrated stable cycling in an all solid-state lithium ion battery utilizing pure $LiBH_4$ as a solid-state electrolyte with $LiCoO_2$ and Li metal as the cathode and anode, respectively.[11] This cell demonstrated a stable reversible capacity of ∼86 mAh/g after 30 cycles when operated at 120 °C with a Li_3PO_4 thin film (∼25 nm) on the $LiCoO_2$ cathode to prevent the highly reducing $LiBH_4$ from reacting with the metal oxide cathode at the electrolyte/cathode interface. On the anode side, recent work has demonstrated that the ionic conductor $LiBH_4$–LiI (3:1 mol ratio) can be used as coating to chemically passivate a $Li_{3.833}Sn_{0.833}As_{0.166}S_4$ solid electrolyte and making it compatible with a metallic Li electrode.[12] This methodology might provide a path forward to solve incompatibility issues observed for other ionic conductors with metallic Li electrodes.

Our group has previously investigated the hydrogen storage properties of a series of complex metal hydride-carbonaceous nanocomposites synthesized by a solvent-assisted mixing method. During these studies it was determined that C_{60} was superior to other carbon nanomaterials in that it facilitated the reformation of the complex metal hydride as well as participated in the hydrogen storage process through the formation of C–H bonds.[13−21] In our examination of the

Received: April 17, 2014
Revised: August 22, 2014
Published: August 29, 2014

dx.doi.org/10.1021/jp503797s | J. Phys. Chem. C 2014, 118, 21755−21761

$LiBH_4$–C_{60} system, we were able to utilize solid state NMR techniques to identify amorphous components of the materials as well as to identify mobile species in the material.[22] Utilizing ^{7}Li NMR, we were able to monitor the fraction of highly mobile lithium species in the nanocomposite. It was determined that the fraction of highly mobile Li^+ in the $LiBH_4$–C_{60} as-prepared (before heating and annealing) material was similar to that found in bulk $LiBH_4$. However, when the material was heated to 300 °C and annealed for 1 h, the fraction of highly mobile species at room temperature was significantly enhanced. After this annealing step at 300 °C, the ^{7}Li spectrum at room temperature is narrower by a factor of 5 when compared to the bulk $LiBH_4$ and as-prepared $LiBH_4$–C_{60} samples. This is similar to the effect observed when $LiBH_4$ is ball milled with lithium halides.[2]

Herein, we investigated the Li ion conducting ability of the $LiBH_4$–C_{60} nanocomposite as a function of temperature and $LiBH_4$ composition to quantify the Li ion conduction in the nanocomposite. We also performed first-principles calculation to understand how C_{60} perturbs the interaction of the lithium cation with the borohydride anion resulting in the observed increase in ionic conductivity.

2. EXPERIMENTAL SECTION

2.1. Materials. Chemicals were used as provided by the supplier and are listed by supplier as follows. Sigma-Aldrich: $LiBH_4$, C_{60}, lithium foil, silicon (~300 mesh), and tetrahydrofuran (THF; anhydrous, inhibitor-free).

2.2. Sample Preparation/Characterization. All manipulations of the samples were performed in an argon-filled glovebox or by utilizing Schlenk line techniques. Samples were prepared by dissolving $LiBH_4$ and C_{60} (~1.0 g total) in 40 mL of THF with stirring for 5–12 h.[18] Solvent was then removed under vacuum and heated (80 °C) on a Schlenk line. The material was lightly ground with a mortar and pestle followed by additional vacuum and heated to remove residual THF. The resultant material is referred to as the "as-prepared" sample (AP). Annealing of the sample was also performed on a Schlenk line. The annealed sample was heated to 300 °C at 5 °C/min and soaked at that temperature for 1 h under Ar flow.

A PerkinElmer Thermogravimetric Analyzer-Pyris 1 TGA was used for thermogravimetric analysis/residual gas analysis (TGA/RGA) experiments. The sample was heated to the desired temperature using a heating rate of 5 °C/min, with a sample size of ~5 mg. The gases released during the heating process were identified using a Hiden Analytical RGA. X-ray powder diffraction (XRD) was performed using a PANalytical X'pert Pro with Cu–Kα radiation, and the samples were protected with a Kapton film to minimize oxidation of the sample.

Pellets of the materials were prepared by pressing the samples in a hydraulic press at 6 tons of pressure under inert conditions. Each pellet (65–85 mg) was 10 mm in diameter with a thickness between 0.8 and 1.1 mm. All electrochemical testing utilized a Swagelok-type cell. Electrochemical testing was performed using a Bio-Logic VMP3 multichannel potentiostat with a frequency response analyzer. Temperature-dependent studies were performed in an oven with the appropriate electrical connections. For the electrochemical impedance spectroscopy (EIS) and constant current cycling experiments, 10 mm diameter lithium foils were utilized in a symmetric cell setup. The EIS was measured in a frequency range of 1 MHz to 100 Hz. The conductivities were obtained from the diameter of a single arc and the intercept on the Z_R axis in the complex impedance plots. Current–voltage (IV) measurements were performed on the pellets to calculate the electrical conductivity of each sample using polished Ni disks as electrodes. For the all-solid-state battery, a 1:1 composite of silicon (~325 mesh):carbon black was pressed onto a nickel foam current collector along with the solid state electrolyte at 6 tons in order to reduce contact resistance between the two. A lithium foil was utilized as the other electrode. The cell was cycled between 0.01 and 1.0 V vs Li at a rate of 0.1C.

2.3. Atomistic Modeling. In order to understand why C_{60} introduction can enhance the conductivity of Li compared to pure $LiBH_4$, we calculated, from first-principles, the binding energy of the Li^+ ion in isolated $LiBH_4$ and that interacting with C_{60}. Our calculations are based on spin polarized density functional theory (DFT) as implemented in Vienna Ab Initio Simulation Package (VASP).[23] In VASP simulations, the generalized gradient approximation (GGA) of exchange correlation functional in the form proposed by Perdew, Burke, and Ernzerhof (PBE)[24] is used. The projector augmented wave (PAW) method[25] with an energy cutoff of 400 eV is adopted. The simulation cell contains vacuum spaces of 12 Å along the x, y, and z directions, in order to avoid interaction between nearest neighbor images. The reciprocal space is represented by the Γ point[26] due to the large simulation cell. All structures are optimized using conjugate gradient method without any symmetric constraints. The convergence criteria of total energy and residual forces on each atom are set to be 1×10^{-4} eV and 0.02 eV/Å, respectively. For charged systems, we also include dipole interaction corrections.[27]

3. RESULTS AND DISCUSSION

TGA and XRD analysis was utilized to understand the changes that occur in the $LiBH_4$–C_{60} system during annealing of the material at 300 °C. The TGA showed that there was a 4.0 wt % loss of H_2 when the sample was heated to 300 °C, followed by an additional loss of 4.7 wt % during annealing of the sample at 300 °C for 1 h for a total mass loss of 8.7 wt %. As shown in Figure 1, a loss of 13.2 wt % was observed upon full desorption of the $LiBH_4$–C_{60} material at 530 °C. This result indicates that the sample annealed at 300 °C remains partially hydrogenated with C_{60}–H bonds and $LiBH_4$, as noted during our previous study.[20] The presence of hydrogen in the nanocomposite after

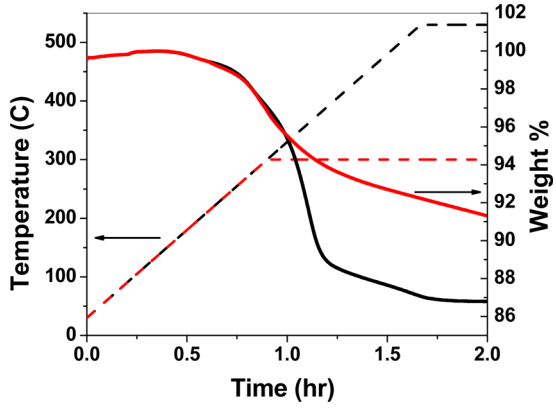

Figure 1. TGA of the $LiBH_4$:C_{60} (70:30) nanocomposite. Fully desorbed material (black) and partially desorbed sample (red). Solid line (TGA) and dash line (temperature). Heating rate is 5 °C/min.

dx.doi.org/10.1021/jp503797s | J. Phys. Chem. C 2014, 118, 21755–21761

annealing is beneficial because in the fully dehydrogenated state, the material has a high electrical conductivity that is not suitable for use as a solid-state electrolyte.

The XRD of the $LiBH_4$−C_{60} nanocomposite was taken in the as-prepared and the annealed (300 °C) state (Figure 2). In the as-prepared state, $LiBH_4$ is present in the low-temperature orthorhombic phase, and even after annealing the sample at 300 °C, $LiBH_4$ remains detectable in the nanocomposite. However, the amount of $LiBH_4$ remaining in the sample is reduced as a result of its partial decomposition in the presence of C_{60} during heating. The presence of crystalline C_{60} was not observed in either sample, which is consistent with results from our previous study of this system.[20] The absence of crystallinity could indicate the presence of defect sites and possibly free volume in this material, which can play a role in the enhanced ion mobility as well.[28,29] Since the diffraction peaks for C_{60} are not present in the XRD, it is presumed that the fullerenes are embedded within the material relatively homogeneously. Since it is known that $LiBH_4$ reduces the fullerenes in this material, $LiBH_4$ molecules around the fullerene are likely to contain defect sites from missing hydrogen. Therefore, the contact area between a $LiBH_4$ crystal and C_{60} would have defects sites and a larger void volume for Li ion conduction. The large amorphous feature at lower 2θ is due to the Kapton film used to cover the sample and prevent oxidation of the sample during analysis.

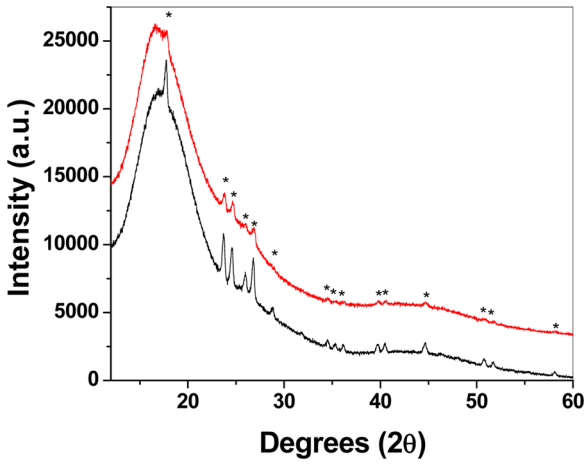

Figure 2. XRD of the $LiBH_4$:C_{60} nanocomposite as-prepared and after annealing at 300 °C for 1 h (black and red, respectively). (*) denotes *orthorhombic*-$LiBH_4$.

EIS was used to measure the ionic conductivity of the $LiBH_4$−C_{60} nanocomposites in the as-prepared and annealed states. A symmetric cell (Li/SSE/Li) setup using two Li foils as electrodes was utilized for these experiments. Pure $LiBH_4$ and $LiBH_4$ that was subject to the same solvent-assisted mixing procedure as the C_{60} containing nanocomposites, were also measured for comparison (see Supporting Information). The Li ionic conductivities of the pure $LiBH_4$ and solvent mixed $LiBH_4$, without C_{60}, were nearly identical and were also consistent with those previously reported. These results indicate that the enhancement of the Li ion mobility is not simply a result of the solvent-assisted mixing process and are in contrast to the observed enhancement of the Li ion mobility in pure $LiBH_4$ after ball-milling.[6] In the as-prepared $LiBH_4$:C_{60} (70:30 and 50:50 wt %) materials, an enhancement in the ionic conductivity is observed at lower temperatures relative to the pure $LiBH_4$ samples. At 40 °C the ionic conductivity of $LiBH_4$ is 2.0×10^{-8} S/cm, while the as prepared $LiBH_4$:C_{60} (50:50 and 70:30 wt %) samples have ionic conductivities of 7.0×10^{-6} and 2.8×10^{-5} S/cm, respectively. The ionic conductivity of each sample increased with increasing temperature to a maximum value of 2.5×10^{-4} and 7.5×10^{-4} S/cm (50:50 and 70:30, respectively) at 140 °C. Electrical conductivity of the samples obtained from the slope of the IV measurements indicates values in electrical conductivity approximately 3 orders of magnitude lower than those obtained for ionic conductivity. As with the ionic conductivity, the electrical conductivity component increases with increasing temperature from 1.2×10^{-9} at 25 °C up to 3.1×10^{-7} at 140 °C for the most electrically conductive sample.

After annealing the as-prepared samples at 300 °C for 1 h, a significant enhancement of the lithium ion mobility is observed, even at room temperature. Ionic conductivities of the annealed samples were 7.2×10^{-5} S/cm and 2.0×10^{-4} (50:50 and 70:30 wt % respectively) at 25 °C. At 140 °C, the ionic conductivity of each sample increased to 2.2×10^{-3} and 6.5×10^{-3} S/cm (50:50 and 70:30 wt %, respectively). Other samples were prepared in which C_{60} was the major component of the nanocomposite (>50 wt %), however, we were unable to successfully press pellets that would not crack or crumble during the experiments. The raw EIS data for the annealed $LiBH_4$:C_{60} 50:50 wt % sample is shown in Figure 3. The complex impedance plot shows only a single arc for the temperatures measured. This behavior was also observed for all of the samples measured. A plot comparing the ionic conductivities (obtained from EIS data) and electrical conductivities (obtained from IV data) of the samples as a function of temperature is shown in Figure 4.

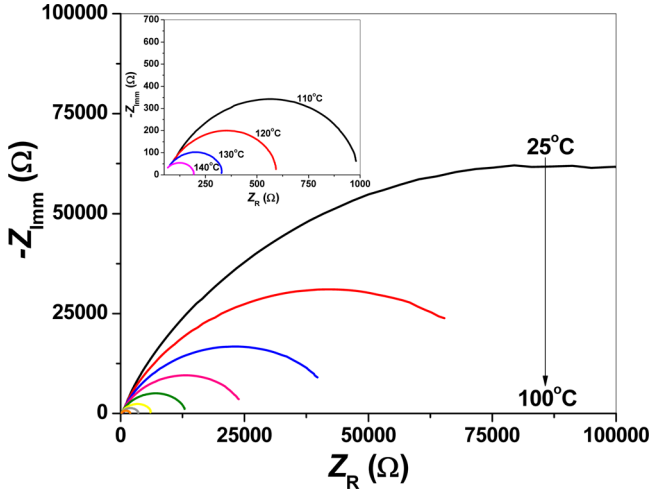

Figure 3. EIS data as a function of temperature for the $LiBH_4$:C_{60} (50:50) annealed at 300 °C pellet utilizing a symmetrical cell set up Li/SSE/Li (SSE= $LiBH_4$ based solid state electrolyte). The sample was first measured at 25 °C, then from 40 to 140 °C in 10 °C increments. The inset shows a zoomed in portion of the high temperature tests.

The activation energy for conduction in each material was also determined from this data in the linear portion of the plot. The activation energy of the pure $LiBH_4$ and $LiBH_4$ subjected to solvent assisted mixing without C_{60} were 0.75 ± 0.03 and 0.74 ± 0.04, respectively, which is close to the low temperature phase (orthorhombic) value of 0.69 eV reported by Orimo.[1] The as prepared and annealed at 300 °C samples prepared with a 70:30 wt % ($LiBH_4$:C_{60}) had activation energies of 0.37 ±

dx.doi.org/10.1021/jp503797s | J. Phys. Chem. C 2014, 118, 21755−21761

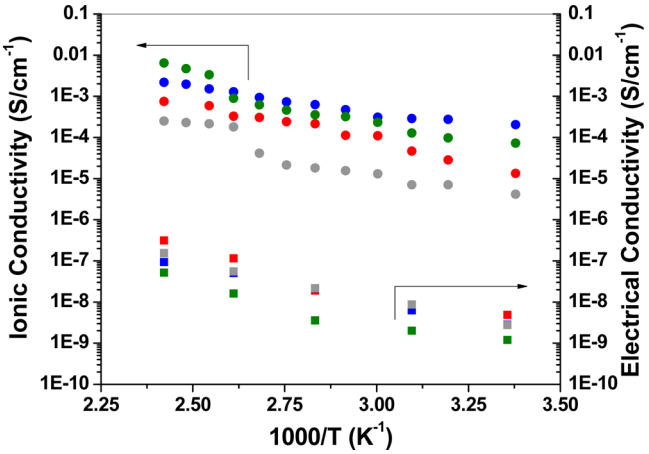

Figure 4. Ionic (●) and electrical (■) conductivity measurements of the $LiBH_4$:C_{60} nanocomposites utilizing a symmetrical cell set up Li/SSE/Li (SSE= $LiBH_4$ based solid state electrolyte). The activation energy for each material was also calculated from this data. Blue - $LiBH_4$:C_{60} (70:30) annealed at 300 °C; green - $LiBH_4$:C_{60} (50:50) annealed at 300 °C; red - $LiBH_4$:C_{60} (70:30) as prepared; gray - $LiBH_4$:C_{60} (50:50) as prepared.

0.02 and 0.29 ± 0.02 eV, respectively. The 50:50 wt % ($LiBH_4$:C_{60}) ratio in as-prepared and annealed at 300 °C samples had activation energies of 0.26 ± 0.03 and 0.23 ± 0.02 eV, respectively. This indicates that the activation energy for ionic conduction of $LiBH_4$ in our materials is significantly lowered in the presence of C_{60}. These values are significantly lower than the activation energy (0.53 eV) observed for the hexagonal phase (high temperature, > 390 K) of $LiBH_4$. The E_a values obtained for the $LiBH_4$−C_{60} nanocomposites are comparable to that observed for lithium borohydride amines $Li_2(BH_4)(NH_2)$ and $Li_4(BH_4)(NH_2)_3$ with E_a values of 0.24 and 0.26 eV, respectively.[9]

Figure 5 shows cycling of the $LiBH_4$−C_{60} nanocomposite in a symmetrical cell and demonstrates the stability of this material versus a pure Li electrode at 25 and 80 °C. The compatibility and stability of our nanocomposite with a pure Li electrode is similar to that observed for β-Li_3PS_4 and indicates

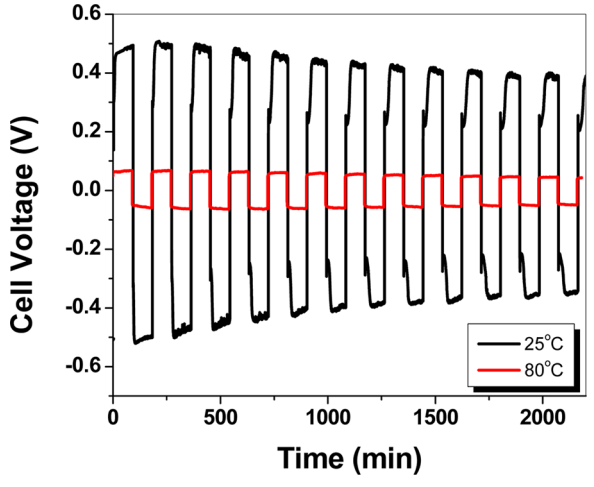

Figure 5. Cycling stability of the $LiBH_4$:C_{60} 300 °C nanocomposite in a symmetrical cell (Li/SSE/Li) with metallic lithium electrodes. The cell was cycled at a current density of 0.1 mA/cm^{-1} at 25 °C (black) and 80 °C (red).

that it could be compatible for use in an all solid state battery utilizing Li metal as the anode.[30]

Figure 6 shows the first two galvanostatic charge/discharge cycles of an all solid-state cell utilizing our solid state electrolyte

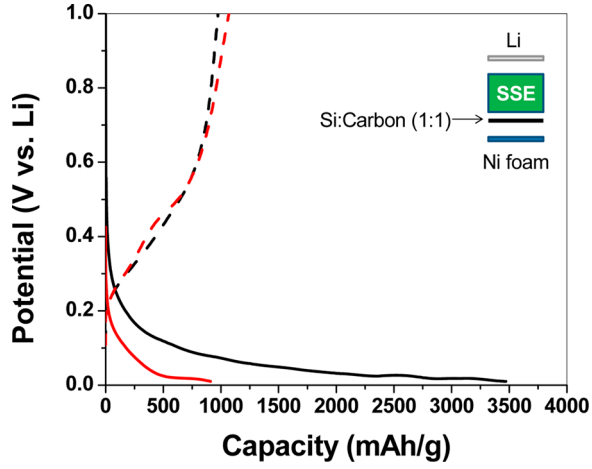

Figure 6. Galvanostatic cycling of an all-solid state cell utilizing silicon as the active anode material with the $LiBH_4$:C_{60} annealed (300 °C) nanocomposite serving as the solid state electrolyte, and lithium metal serving as the cathode (Li/SSE/Si). Cell operated at 80 °C with at a current density of 500 mA/g. 1st cycle (black) and 2nd cycle (red). Inset shows the cell setup of the all solid-state battery.

and silicon as the active anode material at an operating temperature of 80 °C. A first discharge capacity of 3480 mAh/g was observed which corresponds to ∼91% of the theoretical capacity for $Li_{4.4}Si$ (4200 mAh/g); however, only two full cycles were achieved as the cell performance continued to degrade.

This is attributed to the loss in electrical conductivity in the silicon based anode as a result of its large volume expansion (ca. 300%) upon lithiation. Additionally, we were able to incorporate the solid state electrolyte into a full cell (Li/SSE/$LiCoO_2$) and test the cell over multiple cycles. The cell was cycled 5 times at 50 and 80 °C and showed reversible capacities of 8.5 and 10.4 mAh/g, respectively (Supporting Information). This low capacity can be attributed to use of commercially available $LiCoO_2$ on Al foil utilized in the assembly of the cell. It is likely that only the top layers of the $LiCoO_2$ film in contact with the solid electrolyte participated in the electrochemical cycling while the isolated bottom layers were electrochemically inactive. It is also likely that a chemical reaction between the solid electrolyte and the $Li_{1-x}CoO_2$ is occurring at the interface as $LiBH_4$ is still present in the solid-state electrolyte. This reaction will lead to the reduction and deactivation of the transition metal oxide phases.

Recent work describing the reorientations and perturbations on the BH_4^- may provide insight into the mechanism of the observed high ionic conduction.[8,31,32] NMR, neutron vibrational spectroscopy, and quasi-elastic neutron scattering have demonstrated the possibility that the enhanced rotational motion of the BH_4^- results in the enhancement of the Li ion mobility in this system via a "paddle-wheel" mechanism, analogous to that observed for Li_2SO_4.[10,33] In this type of mechanism, the rotating anions promote and assist in the Li cation diffusion jumps resulting in high cationic conductivity. A recent study has also demonstrated that an enhancement in the Na^+ diffusional jump rate and ion mobility is directly related to the rapid reorientation and rotation of $[B_{12}H_{12}]^{2-}$ in

dx.doi.org/10.1021/jp503797s | J. Phys. Chem. C 2014, 118, 21755−21761

$Na_2B_{12}H_{12}$.[34,35] The authors also suggest that the anion to cation size ratio can also play a role in enhancing the ionic mobility because larger anions (i.e., $[B_{12}H_{12}]^{-2}$) can possibly lead to enlarged interstitial diffusion pathways. It is possible that the larger C_{60} molecule in our $LiBH_4$–C_{60} composite, which readily accepts electrons to form stable anions, is behaving in this manner. The calculated diameters of $B_{12}H_{12}^{2-}$ and C_{60} molecules using density functional theory are, respectively, 5.83 and 7.10 Å. As expected, the C_{60} is larger than the $B_{12}H_{12}$ and may be one of the mechanisms involved in the enhancement of Li ion conductivity.

Another possibility is that the C_{60} is partially polymerized (through a reaction with $LiBH_4$) during the solvent assisted mixing/annealing process, resulting in the formation of vacancies and/or channels for translational Li^+ diffusion. This was previously observed for a Li_4C_{60} polymer, which also displayed high ionic conductivity with a low activation energy for Li ion diffusion owing to the two unoccupied Li^+ interstitial sites in voids derived from the octahedral sites.[36]

To gain further insight into the role of C_{60}, we recall our previous NMR studies, which indicate that it interacts with the BH_4^- ion, resulting in a perturbation of the Li^+–BH_4^- bonding. This change in interaction allows for an increase in the Li^+ ion mobility, which explains the observed enhancement in ionic conductivity. The new interface(s) formed from the interaction between the BH_4^- anions and the C_{60} could suggest that nanoionics[37,38] is a potential source of the enhanced ionic mobility observed in this system. In nanoionics, the formation of new interfaces at the nanoscale favors the production of charge carriers, which is typically achieved through the addition of dopants to a lithium based salt. For example, the addition of nano Al_2O_3 and TiO_2 to a LiX (X = I, ClO_4) salt enhanced the ionic conductivity in the bulk material as well as in lithium salt containing polymers.[39−41] This is due to the destabilization and breaking of the ion pairs (Li^+/X^-) of the base lithium salt upon the addition of the proper dopant. The dopant can either adsorb the Li^+ cation or the counteranion to produce vacancies resulting in an enhancement in ionic conduction. The following theoretical analysis of the $LiBH_4$–C_{60} nanocomposite is consistent with this type of nanoionic mechanism.

First-principles calculations show that in the ground state structure of $LiBH_4$, BH_4 forms a tetrahedral pyramid with the Li atom residing under B (Li–B bond length of 1.96 Å). When the Li^+ is removed, the BH_4^- forms a stable cluster with T_d symmetry group. The binding energy between the Li^+ and the BH_4^- cluster ($E_b = E_{Li}^+ + E_{BH4}^- - E_{LiBH4}$) is calculated to be 7.00 eV (Figure 7). However, when C_{60} is introduced, the Li atom prefers to reside on the hollow site atop a pentagonal C ring, forming $LiBH_4$–C_{60} compound. In this case, the binding energy between the Li^+ and the $(C_{60}–BH_4)^-$ cluster ($E_b = E_{Li}^+ + E_{C60\text{-}BH4}^- - E_{C60\text{-}LiBH4}$) is decreased to 5.86 eV, indicating that it is much easier to remove Li^+ from the $LiBH_4$–C_{60} nanocomposite. This is consistent with experimental finding of fast ionic conduction of Li^+ in $LiBH_4$–C_{60}. More interestingly, we observe that once Li^+ is removed, one of the hydrogen atoms from BH_4^- is detached and binds to a C atom in C_{60} cluster, carrying the negative charge with it and forming a hydrogenated C_{60} cluster (C_{60}–H). This is also in agreement with experimental findings where hydrogenated fullerene was detected. Bader's charge analysis[42] reveals that the extra electron of the C_{60}–BH_4^- resides on C_{60}–H (carrying 0.82 e), leaving the BH_3 molecule in almost neutral form (only has 0.18 e). The interaction between the C_{60}–$H^{-0.82}$ and the $BH_3^{-0.18}$ is weak, and the BH_3 can be easily released.

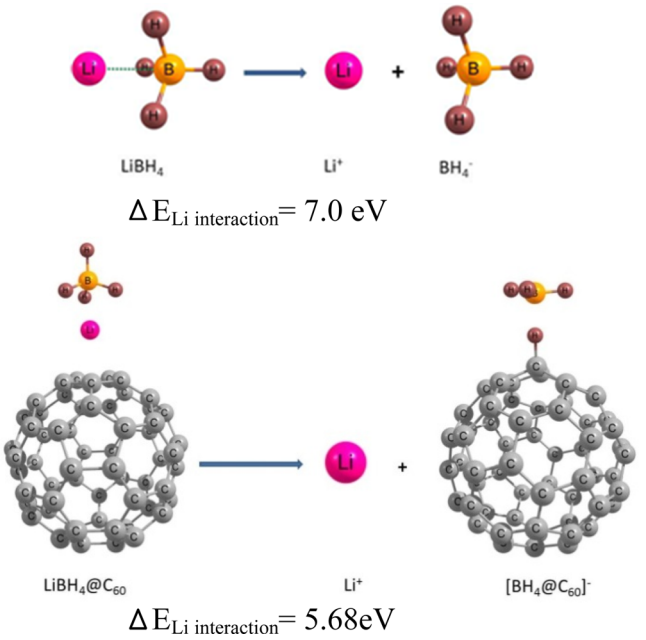

Figure 7. Li interaction in $LiBH_4$ with and without presence of C_{60}.

4. CONCLUSION

In conclusion, we have developed a new $LiBH_4$–C_{60} solid state electrolyte that is capable of being utilized in an all solid-state LIB cell. The activation energy for lithium ion conduction in our nanocomposite is lower than activation energy of lithium ion conduction in pure $LiBH_4$. First-principles calculations show that it is easier to remove Li^+ from $LiBH_4$–C_{60} than from pure $LiBH_4$. Removal of Li^+ allows BH_4^- to interact with C_{60}, eventually hydrogenating it and releasing neutral BH_3. This suggests the possibility that a nanoionic mechanism is responsible for the enhanced ionic mobility in the nanocomposite due to the destabilization/breaking of the Li^+/BH_4^- ion pair in the presence of C_{60}. We have successfully demonstrated that this electrolyte is compatible with a pure lithium metal electrode during extended cycling. The use of C_{60} to enhance the ionic conductivity is a significant departure from the commonly utilized inorganic additives currently used to enhance Li ion mobility in $LiBH_4$ based materials. This methodology could potentially be utilized to enhance alkali-ion mobility in other complex hydrides.

■ ASSOCIATED CONTENT

Supporting Information

Additional electrochemical measurements. This material is available free of charge via the Internet at http://pubs.acs.org.

■ AUTHOR INFORMATION

Corresponding Author

*Mailing address: Savannah River National Laboratory, Clean Energy Directorate, Aiken, SC 29808. Phone: +1 803-646-8876; e-mail: ragaiy.zidan@srnl.doe.gov.

Notes

The authors declare no competing financial interest.

■ ACKNOWLEDGMENTS

Work at SRNL was supported by the U.S. Department of Energy, Office of Science, Basic Energy Sciences, Materials Sciences and Engineering Division. P.A.W. and R.N.C. would like to thank the National Science Foundation grant number DGE0801470, "Sustainable Technology through Advanced Interdisciplinary Research" (STAIR), awarded to the University of Tennessee Knoxville. Research at Virginia Commonwealth University was supported by the U.S. Department of Energy, Office of Basic Energy Sciences, Division of Materials Sciences and Engineering under Award # DE-FG02-96ER45579. We also acknowledge resources of the National Energy Research Scientific Computing Center, which is supported by the Office of Science of the U.S. Department of Energy under Contract No. DE-AC02-05CH11231.

■ REFERENCES

(1) Matsuo, M.; Nakamori, Y.; Yamada, K.; Orimo, S. Lithium Superionic Conduction in Lithium Borohydride Accompanied by Structural Transition. *Appl. Phys. Lett.* **2007**, *91*, 224103.

(2) Maekawa, H.; Matsuo, M.; Takamura, H.; Ando, M.; Noda, Y.; Karahashi, T.; Orimo, S. Halide-Stabilized $LiBH_4$, a Room-Temperature Lithium Fast-Ion Conductor. *J. Am. Chem. Soc.* **2009**, *131*, 894−895.

(3) Matsuo, M.; Takamura, H.; Maekawa, H.; Li, H.-W.; Orimo, S. Stabilization of Lithium Superionic Conduction Phase and Enhancement of Conductivity of $LiBH_4$ by LiCl Addition. *Appl. Phys. Lett.* **2009**, *94*, 084103.

(4) Matsuo, M.; Sato, T.; Miura, Y.; Oguchi, H.; Zhou, Y.; Maekawa, H.; Takamura, H.; Orimo, S. Synthesis and Lithium Fast-Ion Conductivity of a New Complex Hydride $Li_3(NH_2)_2I$ with Double-Layered Structure. *Chem. Mater.* **2010**, *22*, 2702−2704.

(5) Ley, M. B.; Ravnsbæk, D. B.; Filinchuk, Y.; Lee, Y.; Janot, R.; Cho, Y. W.; Skibsted, J.; Jensen, T. R. $LiCe(BH_4)_3Cl$, a New Lithium-Ion Conductor and Hydrogen Storage Material with Isolated Tetranuclear Anionic Clusters. *Chem. Mater.* **2012**, *24*, 1654−1663.

(6) Sveinbjörnsson, D.; Myrdal, G. J. S.; Blanchard, D.; Bentzen, J. J.; Hirata, T.; Mogensen, M. B.; Norby, P.; Orimo, S.; Vegge, T. Effect of Heat Treatment on the Lithium Ion Conduction of the $LiBH_4$−LiI Solid Solution. *J. Phys. Chem. C* **2013**, *117*, 3249−3257.

(7) Yamauchi, A.; Sakuda, A.; Hayashi, A.; Tatsumisago, M. Preparation and Ionic Conductivities of $(100 - x)(0.75Li_2S\cdot 0.25P_2S_5)\cdot xLiBH_4$ Glass Electrolytes. *J. Power Sources* **2013**, *244*, 707−710.

(8) Verdal, N.; Udovic, T. J.; Rush, J. J. The Nature of BH_4^- Reorientations in Hexagonal $LiBH_4$. *J. Phys. Chem. C* **2012**, *116*, 1614−1618.

(9) Matsuo, M.; Remhoff, A.; Martelli, P.; Caputo, R.; Ernst, M.; Miura, Y.; Sato, T.; Oguchi, H.; Maekawa, H.; Takamura, H.; et al. Complex Hydrides with $(BH_4)^-$ and $(NH_2)^-$ Anions as New Lithium Fast-Ion Conductors. *J. Am. Chem. Soc.* **2009**, *131*, 16389−16391.

(10) Matsuo, M.; Orimo, S. Lithium Fast-Ionic Conduction in Complex Hydrides: Review and Prospects. *Adv. Energy Mater.* **2011**, *1*, 161−172.

(11) Takahashi, K.; Hattori, K.; Yamazaki, T.; Takada, K.; Matsuo, M.; Orimo, S.; Maekawa, H.; Takamura, H. All-Solid-State Lithium Battery with $LiBH_4$ Solid Electrolyte. *J. Power Sources* **2013**, *226*, 61−64.

(12) Sahu, g.; Lin, z.; Li, J.; Liu, Z.; Dudneyb, N.; Liang, C. Air-Stable, High-Conduction Solid Electrolytes of Arsenic-Substituted Li_4SnS_4. *Energy Environ. Sci.* **2014**, *7*, 1053−1058.

(13) Teprovich, J. A. J.; Knight, D. A.; Peters, B.; Zidan, R. Comparative Study of Reversible Hydrogen Storage in Alkali-Doped Fulleranes. *J. Alloys Compd.* **2013**, *580*, S364−S367.

(14) Teprovich, J. A., Jr.; Knight, D. A.; Wellons, M. S.; Zidan, R. Catalytic Effect of Fullerene and Formation of Nanomcomposites with Complex Hydrides: $NaAlH_4$ and $LiAlH_4$. *J. Alloys Compd.* **2011**, *509S*, S562−S566.

(15) Teprovich, J. A., Jr.; Wellons, M.; Lascola, R.; Hwang, S.; Ward, P.; Compton, R.; Zidan, R. Synthesis and Characterization of a Lithium Doped Fullerane (Li_x−C_{60}−H_y) for Reversible Hydrogen Storage. *Nano Lett.* **2012**, *12*, 582−589.

(16) Paolone, A.; Palumbo, O.; Leardini, F.; Cantelli, R.; Knight, D. A.; Teprovich, J. A., Jr; Zidan, R. A Spectroscopic Investigation of Hydrogenated Li Doped Fullerane. *J. Alloys Compd.* **2013**, *580*, S67−S69.

(17) Paolone, A.; Vico, F.; Teocoli, F.; Sanna, S.; Palumbo, O.; Cantelli, R.; Knight, D. A.; Teprovich, J. A., Jr.; Zidan, R. Relaxation Processes and Structural Changes in Li and Na Doped Fulleranes for Hydrogen Storage. *J. Phys. Chem. C* **2012**, *116*, 16365−16370.

(18) Wellons, M. S.; Berseth, P. A.; Zidan, R. Novel Catalytic Effects of Fullerene for $LiBH_4$ Hydrogen Uptake and Release. *Nanotechnology* **2009**, *20*, 204022.

(19) Knight, D. A.; Teprovich, J. A., Jr.; Summers, A.; Peters, B.; Ward, P. A.; Compton, R. N.; Zidan, R. Synthesis, Characterization, and Reversible Hydrogen Sorption Study of Sodium-Doped Fullerene. *Nanotechnology* **2013**, *24*, 455601.

(20) Ward, P.; Teprovich, J. A. J.; Peters, B.; Wheeler, J.; Compton, R. N.; Zidan, R. Reversible Hydrogen Storage in a $LiBH_4$-C_{60} Nanocompsite. *J. Phys. Chem. C* **2013**, *117*, 22569−22575.

(21) Wang, Q.; Jena, P. Density Functional Theory Study of the Interaction of Hydrogen with Li_6C_{60}. *J. Phys. Chem. Lett.* **2012**, *3*, 1084−1088.

(22) Shane, D. T.; Corey, R. L.; Rayhel, L. H.; Wellons, M. S.; Teprovich, J. A., Jr; Zidan, R.; Hwang, S.; Bowman, R.C., Jr; Conradi, M. S. NMR Study of $LiBH_4$ with C_{60}. *J. Phys. Chem. C* **2010**, *114*, 19862−19866.

(23) Kresse, G.; Heffner, J. Efficient Iterative Schemes for Ab Initio Total-Energy Calculations Using a Plane-Wave Basis Set. *Phys. Rev. B* **1996**, *54*, 11169.

(24) Perdew, J. P.; Burke, K.; Ernzerhpf, M. Generalized Gradient Approximation Made Simple. *Phys. Rev. Lett.* **1996**, *77*, 3865−3868.

(25) Bloechl, P. E. Projector Augmented-Wave Method. *Phys. Rev. B* **1994**, *50*, 17953−17979.

(26) Monkhorst, H. J.; Pack, J. D. Special Points for Brillouin-Zone Integrations. *Phys. Rev. B* **1976**, *13*, 5188−5192.

(27) Makov, G.; Payne, M. C. Periodic Boundary Conditions in Ab Initio Calculations. *Phys. Rev. B* **1995**, *51*, 4014−4022.

(28) Turnbull, D.; Cohen, M. H. Free-Volume Model of the Amorphous Phase: Glass Transition. *J. Chem. Phys.* **1961**, *34*, 120−131.

(29) Cohen, M. H.; Turnbull, D. Molecular Transport in Liquids and Glasses. *J. Chem. Phys.* **1959**, *31*, 1164−1173.

(30) Liu, Z.; Fu, W.; Payzant, E. A.; Yu, X.; Wu, Z.; Dudney, N. J.; Kiggans, J.; Hong, K.; Rondinone, A. J.; Liang, C. Anomalous High Ionic Conductivity of Nanoporous β-Li_3PS_4. *J. Am. Chem. Soc.* **2013**, *135*, 975−978.

(31) Verdal, N.; Udovic, T. J.; Rush, J. J.; Liu, X.; Majzoub, E. H.; Vajo, J. J.; Gross, A. F. Dynamical Perturbations of Tetrahydroborate Anions in $LiBH_4$ due to Nanoconfinement in Controlled-Pore Carbon Scaffolds. *J. Phys. Chem. C* **2013**, *117*, 17983−17995.

(32) Verdal, N.; Udovic, T. J.; Rush, J. J.; Wu, H.; Skripov, A. V. Evolution of the Reorientational Motions of the Tetrahydroborate Anions in Hexagonal $LiBH_4$−LiI Solid Solution by High-Q Quasielastic Neutron Scattering. *J. Phys. Chem. C* **2013**, *117*, 12010−12018.

(33) Lunden, A. Evidence For and Against the Paddle-Wheel Mechanism of Ion Transport in Superionic Sulphate Phases. *Solid State Commun.* **1988**, *65*, 1237−1240.

(34) Skripov, A. V.; Babanova, O. A.; Soloninin, A. V.; Stavila, V.; Verdal, N.; Udovic, T. J.; Rush, J. J. Nuclear Magnetic Resonance Study of Atomic Motion in $A_2B_{12}H_{12}$ (A = Na, K, Rb, Cs): Anion Reorientations and Na^+ Mobility. *J. Phys. Chem. C* **2013**, *117*, 25961−25968.

(35) Udovic, T. J.; Matsuo, M.; Unemoto, A.; Verdal, N.; Stavila, V.; Skripov, A. V.; Rush, J. J.; Takamurag, H.; Orimo, S. Sodium Superionic Conduction in $Na_2B_{12}H_{12}$. *Chem. Commun.* **2014**, *50*, 3750−3752.
(36) Ricco, M.; Belli, M.; Mazzani, M.; Pontirolo, D.; Quintavalle, D.; Janossy, A. Superionic Conductivity in the Li_4C_{60} Fulleride Polymer. *Phys. Rev. Lett.* **2009**, *102*, 145901.
(37) Maier, J. Pushing Nanoionics to the Limits: Charge Carrier Chemistry in Extremely Small Systems. *Chem. Mater.* **2014**, *26*, 348−360.
(38) Maier, J. Nanoionics: Ionic Charge Carriers in Small Systems. *Phys. Chem. Chem. Phys.* **2009**, *11*, 3011−3022.
(39) Liang, C. C. Conduction Characteristics of the Lithium Iodide−Aluminum Oxide Solid Electrolytes. *J. Electrochem. Soc.* **1973**, *12*, 1289−1292.
(40) Croce, F.; Appetecchi, G. B.; Persi, L.; Scrosati, B. Nanocomposite Polymer Electrolytes for Lithium Batteries. *Nature* **1998**, *394*, 456−458.
(41) Weiczorek, W.; Florjanczyk, Z.; Stevens, J. R. Composite Polyether Based Solid Electrolytes. *Electrochim. Acta* **1995**, *40*, 2251−2258.
(42) Tang, W.; Sanville, E.; Henkelman, G. A Grid-Based Bader Analysis Algorithm without Lattice Bias. *J. Phys.: Condens. Matter* **2009**, *21*, 084204−084210.

Experimental and Theoretical Analysis of Fast Lithium Ionic Conduction in a $LiBH_4$-C_{60} Nanocomposite

Joseph A. Teprovich Jr.,[†] Héctor R. Colón-Mercado,[†] Patrick A. Ward,[†‡] Brent Peters,[†] Santanab Giri,[^] Jian Zhou,[^] Scott Greenway,[§] Robert N. Compton,[‡] Purusottan Jena,[^] and Ragaiy Zidan*[†]

[†] Savannah River National Laboratory, Clean Energy Directorate, Aiken, SC 29808, USA
[‡] Department of Chemistry, University of Tennessee, Knoxville, TN 37996, USA
^ Virginia Commonwealth University, Physics Department, Richmond, VA 23284, USA
§ 301 Gateway, Dr., Aiken, SC 29808, USA

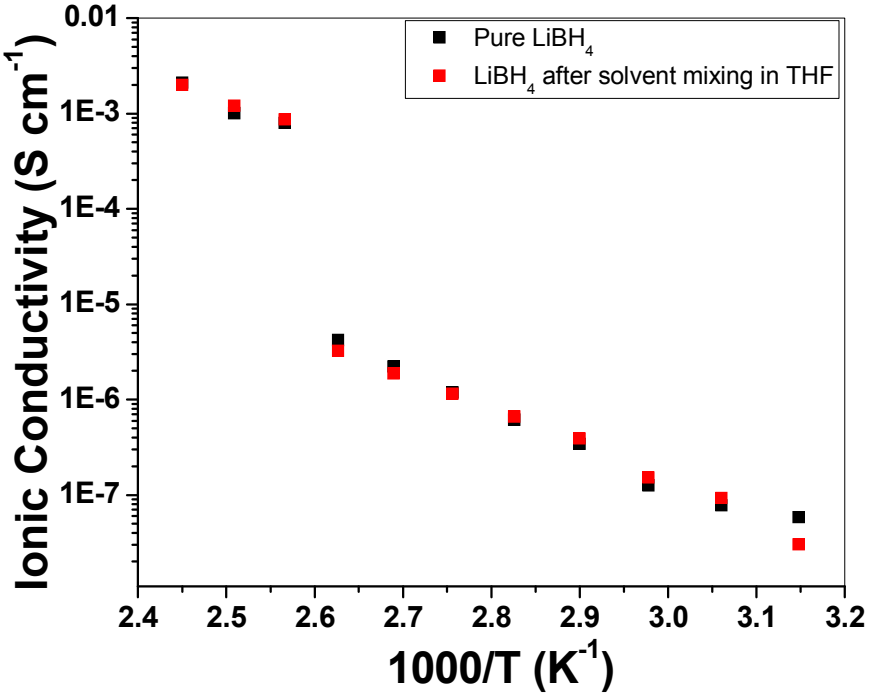

Figure S1. Ionic conductivity data for the pure $LiBH_4$ (black) and $LiBH_4$ sample that was subject to the same solvent assisted mixing process as the C_{60} containing nanocomposites. The values obtained match that previously reported for $LiBH_4$ and indicates that the solvent assisted mixing process is not responsible for the observed enhanced conductivity.

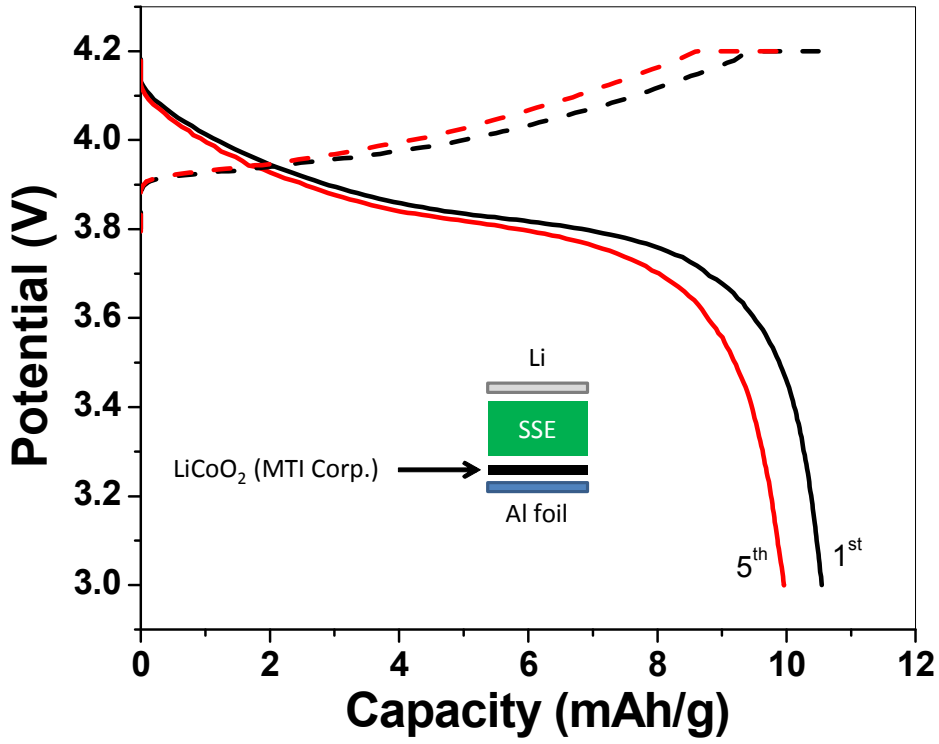

Figure S2. Cycling of an all solid-state cell utilizing a commercial $LiCoO_2$ film as the cathode, lithium foil as the anode, and the $LiBH_4$-C_{60} as the solid state electrolyte. The 1st cycle is shown in black and the 5th cycle is shown in red. The solid line is the discharge and the dash line is the charging step. The cell was cycled at ±0.05 mA between 3.0-4.2V. After the constant current charging of the cell, a constant voltage charging step at 4.2V was performed with a cut-off current of 0.01mA. Cycling was performed at 80°C. Inset shows the cell set-up.

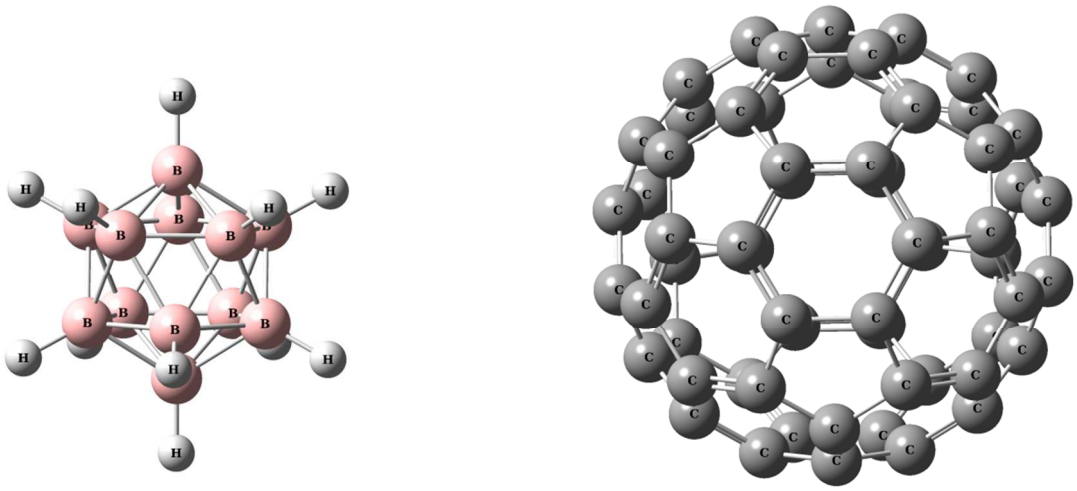

(a) (b)

Figure S3. Empirical optimization of the species (a) $B_{12}H_{12}^{2-}$ and (b) C_{60}.